symmetry

IMPACT FACTOR 2.2

CITESCORE 5.3

Article

The Origin of Dark Matter and Dark Energy: Covarying Coupling Constants?

Rajendra P. Gupta

Special Issue

Nature and Origin of Dark Matter and Dark Energy, 2nd Edition

Edited by

Dr. Vesselin Gueorguiev and Prof. Dr. Enrique Gaztanaga

MDPI

https://doi.org/10.3390/sym18020300

symmetry

MDPI

Article

The Origin of Dark Matter and Dark Energy: Covarying Coupling Constants?

Rajendra P. Gupta

Department of Physics, University of Ottawa, Ottawa, ON K1N 6N5, Canada; rgupta4@uottawa.ca

Abstract

We show that the FLRW metric, modified to include interrelated variation in the speed of light and gravitational constants, leads to Friedmann equations containing terms that behave like dark matter and dark energy without the cosmological constant. When we permit tired light (TL) to contribute to the redshift due to the expanding universe, thus defined by covarying coupling constants (CCCs), the resulting CCC+TL model has a critical density that is just enough to account for the baryon matter in the universe. The CCC+TL cosmology model is consistent with all of the observations that we had the time and the resources to study, including BAOs (baryon acoustic oscillations), the CMB (cosmic microwave background) sound horizon angular size, the time dilation effect, galaxy formation time scales at cosmic dawn, galaxy rotation curves, gravitational lensing, galaxy cluster and ultra-faint dwarf galaxy dynamics, and the mass, size, density, and luminosity evolution of galaxies. We briefly review them in this paper. Additionally, the new model does not suffer from the coincidence problem of the ΛCDM model and complies with the recent DESI findings of an increasing dark energy density with redshift. We present the fundamentals of the CCC+TL model and discuss its applications to some decisive observations. We have considered temporal variation in the constant for cosmological studies and their spherically symmetric variation in astrophysical situations. We conclude that the illusion of dark matter and dark energy in cosmological and astrophysical observations originates from CCC.

Keywords: dark energy; dark matter; Dirac cosmology; tired light; varying coupling constants

1. Introduction

Dark matter and dark energy are the foundational pillars of the most accepted cosmology, that of the Lambda Cold Dark Matter (ΛCDM). The concept of dark matter originated from the observation of the dynamics of stars in galaxies and the dynamics of galaxies in galaxy clusters. It was found that the mass of the visible matter was too small to keep the objects gravitationally bound to the mass structures studied, leading to the conclusion that there must be invisible matter, i.e., dark matter, providing the required additional gravitational force [1–3]. The concept of dark energy has its origin in Einstein's equations of general relativity, where Einstein [4] introduced the Λ constant to prevent the universe from collapsing under the gravitational pull of matter and to be compliant with the perfect cosmological principle—the universe is the same for all observers everywhere in the universe and *at all times*. It was abandoned by Einstein and others but was reintroduced after it was noticed by studying the luminosity–distance–redshift relations of type 1a supernovae standard candles that the universe expansion rate was accelerating [5,6], rather than

Academic Editors: Giuseppe Latino, Vesselin Gueorguiev and Enrique Gaztanaga

Received: 12 October 2025
Revised: 27 November 2025
Accepted: 15 December 2025
Published: 6 February 2026

decelerating as expected prior to the launch of the Hubble Space Telescope in the 1990s. We may thus consider that the Hubble Space Telescope was pivotal in the development of modern cosmology, specifically the ΛCDM model. In this model, the matter density turned out to be many times greater than the baryon density following observations and thus it was considered the cosmological evidence of dark matter.

The origins of dark matter and dark energy remain elusive even today. The most prevalent idea for the origin dark matter is that it comprises elementary particles that do not interact with normal matter and radiation, except gravitationally. Other ideas are based on modifying the Newtonian [7] and general relativity theories of gravitation, as well as that of evolutionary coupling constants [8], to account for the observations attributed to dark matter. Milgrom's concept of modified Newtonian dynamics (MOND), the most studied alternative to dark matter, has recently been reviewed by Desmond [9] for its successes and failures in various astrophysical applications.

Other such theories that are replacing dark matter and dark energy include the relativistic generalization of MOND in the form of tensor–vector–scalar gravity (TeVeS) [10], f(R) gravity [11], negative mass, dark fluid [12], entropic gravity [13], the dark dimension (e.g., [14]), retarded gravity (e.g., [15,16]), and others (e.g., [17,18]). The criticism that such theories are not in compliance with the CMB anisotropy and matter power spectra observations has been refuted by Skordis and Złośnik [19]. Roberts et al. [20] used the gravothermal collapse of self-interacting dark matter to explain several galaxy rotation curves that were considered outliers in earlier studies. Mistele et al. [21] analyzed the gravitational potentials derived from gravitational lensing of isolated galaxies, that imply rotation curves remain flat up to a few hundred kpc [22]. They showed that such curves may extend to the Mpc scale. These findings may imply that the galaxy halo is in thermal equilibrium even at larger radii, where particles do not have time to relax [23]. The universality of dark matter has been challenged by a new class of dark matter-free dwarf galaxies, raising concerns about galaxy formation models within the ΛCDM paradigm [24].

It is worth considering the f(R) gravity theory a little further. In exploring alternatives to dark matter and dark energy, recent tests of modified gravity using astrometric data provide valuable insight. Jovanovic et al. [25] showed that f(R) gravity can reproduce the Fundamental Plane of elliptical galaxies without invoking dark matter, illustrating the capacity of such models to account for galactic dynamics through geometric modifications of gravity. More recently, Jovanovic et al. [26] extended this framework to spiral systems, successfully recovering the baryonic Tully–Fisher relation under the same theoretical assumptions. In a broader context, 'The CosmoVerse White Paper' [27] discussed the ongoing observational tensions in ΛCDM cosmology, examining how systematic effects and extensions to fundamental physics may reconcile these discrepancies. Collectively, these works highlight the importance of empirical tests of modified gravity across multiple astrophysical regimes for reassessing the standard cosmological paradigm.

The origin of dark energy is considered to be associated with the concept of vacuum energy from quantum field theory, except for the fact that the two differ hugely in their magnitude. Many alternatives to it have also been suggested, such as modified theories of gravity (e.g., [28–30]; [31]—review), the black holes effect (e.g., [32–37]), string theory (e.g., [38,39]), and evolutionary coupling constants (e.g., [40,41]).

Since extensive literature exists on the theories and observations related to dark matter and dark energy, we will refrain from covering the subject further. Instead, we will focus, in this work, on studying the interrelated evolution of coupling constants, i.e., the concept of covarying coupling constants, and how they manifest as dark matter and dark energy in cosmological and astrophysical observations. Essentially, we present a case for dark matter and dark energy originating from the covarying coupling constants in the generalized

Dirac cosmology (e.g., [42–44])—Dirac conceptualized the variation in gravitational and fine-structure constants with cosmic expansion based on his large number hypothesis [45] and Gupta [46] generalized it to all the constants, as reasoned by Uzan [47].

Our focus in this paper is to show how our work in cosmology and astrophysics to date presents a case for CCCs to be the origin for dark matter and dark energy. Thus, this paper is not intended to review our earlier published work in any detail; it just provides their snippets with citations and presents some new results. To keep our focus, we heavily rely on our earlier work through citations and avoid distraction by minimizing details already provided in such citations. The current section is followed by Section 2 presenting CCC phenomenology, Section 3 evaluating its cosmological test, Section 4 assessing its astrophysical test, Section 5 discussing the findings of the paper, and Section 6 narrating the conclusions.

2. CCC Phenomenology

The premise of this study is the idea that if fundamental coupling constants evolve, they do so interdependently via a shared dimensionless function, $f(t)$. Based on local energy conservation principles in stellar explosions, constants such as the speed of light (c), gravitational constant (G), Planck constant ($\hbar$), and Boltzmann constant (k_B) are hypothesized to vary as $c(t) = c_0 f(t)$, $G(t) = G_0 f(t)^3$, $\hbar(t) = \hbar_0 f(t)^2$, and $k_B(t) = k_{B0} f(t)^2$, where the subscript 0 indicates the value at the current epoch t_0 [46]. Dimensional analysis suggests this variation is linked to the length dimension of each constant. Since the length unit itself is defined by the speed of light, it must also evolve according to $length(t) = length_0 f(t)$. While $f(t)$ is not strictly defined and could theoretically be unity (implying constants are constants), it must be well behaved and equal to unity at $t = t_0$. Adhering to Occam's razor, we adopt $f(t) = \exp(\alpha(t - t_0))$, where α is a constant to be determined empirically. This choice simplifies the modified Einstein and Friedmann equations in comparison to the ΛCDM model, though we acknowledge that $f(t)$ could technically be more complex, such as by adapting to phase transitions as the universe evolves and be spatially varying.

The covarying coupling constants (CCCs) framework is rooted in Dirac cosmology, specifically Dirac's hypothesis of evolving gravitational and fine-structure constants, and Uzan's deduction that variation in one dimensionful constant necessitates variation in others. Note that dimensionless constants, such as the fine-structure constant, do not fall under the CCCs principle.

The conceptual roots of the CCCs framework lie in Dirac's [45] proposal of correlated variations in gravitational and electromagnetic coupling strengths and in subsequent developments by Gilbert [42,43] and Canuto & Londenquai [44], who explored the cosmological implications of evolving constants in generalized Dirac cosmology. Since then, several authors have advanced mathematically similar ideas. In particular, Bouvier (as reviewed by Maeder and Gueorguiev [48,49]) and Maeder [50] have developed scale-invariant vacuum cosmological models in which the gravitational coupling, as well as the fine-structure constant, effectively vary with cosmic time through a Weyl-integrable rescaling of the metric. Although their theoretical motivations differ, both approaches introduce a nontrivial time dependence of gravitational strength that has consequences resembling those emerging from the CCC modifications to the Friedmann equations. The present work extends this conceptual line by showing that the correlated variations of all dimensionful constants, governed by a single function $f(t)$, naturally generate terms that behave like dark matter and dark energy in cosmological and astrophysical contexts.

Time-varying-G frameworks have also been extensively studied in scalar–tensor theories, most notably in Jordan–Brans–Dicke (JBD) gravity [51]. While the CCCs model shares the general feature of a dynamical gravitational coupling, its structure differs fundamentally

from JBD models: with CCCs the variations of G, c, h, and other constants are not mediated by a scalar field with a kinetic term, but are instead determined phenomenologically through dimensional analysis and local energy conservation, leading to a distinct modification of the Einstein–Friedmann equations. A related class of theories—Weyl-integrable geometry [44,52,53]—also employs a non-metric connection to produce effective rescalings of physical units. Although a CCCs model does not invoke non-metricity or Weyl gauge symmetry, the resulting behavior of gravitational coupling shares superficial similarities with Weyl-integrable spacetime models. The present comparison highlights that the CCCs model occupies a complementary theoretical space; it is neither a scalar–tensor theory in the JBD sense, nor a Weyl-integrable geometric modification, but a phenomenological framework in which correlated variations in dimensionful constants reproduce the effects attributed to dark matter and dark energy. A more detailed theoretical elaboration has been provided in Cuzinatto et al. [54], where an action-based formulation relating $c(t)$ and $G(t)$ was developed.

Extensive literature exists constraining the variation of G (e.g., [55–79]), c [80–89], and other dimensionful constants. However, these studies generally assume one constant varies while fixing the others, which effectively forces $f(t) = 1$ a priori. By fixing $f(t)$, all CCCs are constrained to their current values, making the measurement of single-constant variation meaningless [46].

The CCCs concept requires modifying the FLRW metric and the Einstein equations, which yields altered Friedmann equations [8]. We reiterate the relevant equations here from prior work for completeness [40,41]. Since $c \sim f(t)$ and r and $dr \sim f(t)$, the FLRW metric is

$$ds^2 = c_0^2 dt^2 f(t)^2 - a(t)^2 f(t)^2 \left(\frac{dr^2}{1-\kappa r^2} + r^2 \left(d\theta^2 + \sin^2\theta d\phi^2, \right) \right) \tag{1}$$

the modified Friedmann equations are

$$\left(\frac{\dot{a}}{a} + \alpha \right)^2 = \frac{8\pi G_0}{3c_0^2}\varepsilon - \frac{\kappa c_0^2}{a^2}, \text{ and} \tag{2}$$

$$\frac{\ddot{a}}{a} = -\frac{4\pi G_0}{3c_0^2}(\varepsilon + 3p) - \alpha \left(\frac{\dot{a}}{a}, \right) \tag{3}$$

and the modified continuity equation is

$$\dot{\varepsilon} + 3\frac{\dot{a}}{a}(\varepsilon + p) = -\alpha(\varepsilon + 3p). \tag{4}$$

Here, the scale factor $a(t)$ accounts for the macroscopic expansion in the universe's size, the function $f(t)$ may be considered the microscopic expansion of the length unit itself, κ is the curvature constant, ε is the energy density of all the components, and p is their pressure. Also, $\alpha = \dot{f}/f$. Writing $p = \varepsilon w$, the solution of Equation (4) is (recall that $w = 0$ for matter, and w $= 1/3$ for radiation),

$$\varepsilon = \varepsilon_0 a^{-3(1+w)} f^{-(1+3w)}. \tag{5}$$

Defining the Hubble expansion parameter as $H \equiv \dot{a}/a$, we may write Equation (2) for a flat universe ($\kappa = 0$) as

$$(H + \alpha)^2 = \frac{8\pi G_0}{3c_0^2}\varepsilon \Rightarrow \varepsilon_{c,0}^C \equiv \frac{3c_0^2(H_0 + \alpha)^2}{8\pi G_0}. \tag{6}$$

Equation (6) establishes the universe's critical density $\varepsilon^C_{c,0}$ for the CCCs model, which depends on both the Hubble constant and the parameter α. To ensure the density remains non-negative, the condition $\alpha \geq -H$ is required. From Equations (5) and (6)

$$(H+\alpha)^2 = (H_0+\alpha)^2\left(\Omega^C_{m,0}a^{-3}f^{-1} + \Omega^C_{\mathrm{r},0}a^{-4}f^{-2}\right). \tag{7}$$

Here, $\Omega^C_{m,0} \equiv \varepsilon_{m,0}/\varepsilon^C_{c,0}$ is the relative matter energy density and $\Omega_{\mathrm{r},0} \equiv \varepsilon^C_{r,0}/\varepsilon^C_{c,0}$ is the relative radiation energy density. However, we may expand and rewrite Equation (2) as

$$\begin{aligned} H^2 &= \tfrac{8\pi G_0}{3c_0^2}\varepsilon - \alpha^2 - 2\alpha H \\ &= \tfrac{8\pi G_0}{3c_0^2}\varepsilon - \alpha^2 - 2\alpha\left(\left(\tfrac{8\pi G_0}{3c_0^2}\varepsilon\right)^{1/2} - \alpha\right) \end{aligned} \tag{8}$$

$$= \frac{8\pi G_0}{3c_0^2}\varepsilon + \alpha^2 - 2\alpha\left(\frac{8\pi G_0}{3c_0^2}\varepsilon\right)^{1/2} = \frac{8\pi G_0}{3c_0^2}\left(\varepsilon + \frac{3c_0^2}{8\pi G_0}\alpha^2 - 2\alpha\left(\frac{3c_0^2}{8\pi G_0}\right)^{-1/2\ \ 1/2}\varepsilon\right) \equiv \frac{8\pi G_0}{3c_0^2}(\varepsilon + \varepsilon_{\alpha e} + \varepsilon_{\alpha m}). \tag{9}$$

Here, ε is the composite energy density of matter and radiation. Since the second and the third terms both emerge from α, we have labeled them accordingly: $\varepsilon_{\alpha e}$ as the α-energy density and $\varepsilon_{\alpha m}$ as the α-matter energy density. As α turns out to be negative, the contribution of α-matter is positive. In terms of the standard definition of the critical density $\varepsilon^S_{c,0} \equiv 3c_0^2H_0^2/8\pi G_0$; Equation (9) becomes

$$H^2 = H_0^2(\Omega^S_{m,0}a^{-3}f^{-1} + \Omega^S_{\mathrm{r},0}a^{-4}f^{-2} + \Omega^S_{\alpha e} + \Omega^S_{\alpha m,0}a^{-3/2}f^{-1/2}\Big). \tag{10}$$

Let us compare it with similar expressions for the ΛCDM model in a flat universe:

$$H^2 = \frac{8\pi G_0}{3c_0^2}\varepsilon + \frac{\Lambda}{3} = \frac{8\pi G_0}{3c_0^2}\left(\varepsilon + \frac{c_0^2}{8\pi G_0}\Lambda\right) \equiv \frac{8\pi G_0}{3c_0^2}(\varepsilon + \varepsilon_\Lambda) = H_0^2(\Omega_{m,0}a^{-3} + \Omega_{\mathrm{r},0}a^{-4} + \Omega_\Lambda) \tag{11}$$

Comparing the above equations, we find that the cosmological constant termed $\Lambda/3$ in the ΛCDM model is replaced by the constant α^2 in the CCCs model. Since dark energy is considered to be associated with Λ, we may consider that it originated from the covarying coupling constant α, i.e., *dark energy is a manifestation of covarying coupling constants*. Additionally, there is an evolutionary term $-2\alpha\left(8\pi G_0\varepsilon/3c_0^2\right)^{1/2}$. This term (positive, since α is negative) may be considered a dynamic component of the quintessence (time-varying dark energy), as a dark matter component that evolves differently than baryonic matter, or as something yet to be specified.

Since $(H+\alpha)^2 = H^2 + 2H\alpha + \alpha^2$, we can rewrite it as

$$H^2 = (H+\alpha)^2 + \alpha^2 - 2\alpha(H+\alpha). \tag{12}$$

Dividing it by H_0^2 and comparing it with Equation (10), we may write at the current time (since $\Omega^S_{m,0} \gg \Omega^S_{r,0}$)

$$1 = \frac{(H_0+\alpha)^2}{H_0^2} + \frac{\alpha^2}{H_0^2} - \frac{2\alpha(H_0+\alpha)}{H_0^2} \equiv \Omega^S_{bm,0} + \Omega^S_{\alpha e} + \Omega^S_{\alpha m,0} = \Omega^S_{bm,0} + \Omega^S_{\alpha e} + 2\sqrt{\Omega^S_{\alpha e}\Omega^S_{bm,0}}. \tag{13}$$

We have labeled the first term as *bm* as it represents only the baryonic matter in the CCC+TL model [40,41].

Defining a new parameter $X = -\alpha/H_0$ in the CCCs model ($X = -\alpha/H_x$ in the CCC+TL model), we may write Equation (13) as

$$1 = (1-X)^2 + X^2 + 2X(1-X). \tag{14}$$

Thus, $\Omega^S_{bm,0} \equiv (1-X)^2$, $\Omega^S_{\alpha e} \equiv X^2$, and $\Omega^S_{\alpha m,0} \equiv 2X(1-X)$. Here, all three terms represent energy densities relative to the critical density. Since all the energy densities must be positive, $2X(1-X)$ can only be positive when $0 \leq X \leq 1$. The first and last terms on the right-hand side of Equations (13) and (14), $\Omega_{bm,0}$ and $\Omega_{\alpha m,0}$ $\left(= 2\sqrt{\Omega_{\alpha e,0}\Omega_{bm,0}}\right)$, contain baryonic components and thus are directly affected by gravitation. Therefore, X, and also α, can change locally due to the baryon accretion under gravitational force. X is similar to energy densities considered constant at *cosmological* scales, such as the critical density, but drastically different at the *astrophysical* scales of stars and galaxies. In high-baryon-density regions, only baryons exist, i.e., $X = 0$. At the maximum possible value of $X = 1$, only α-energy exists. When $0 < X(r,\theta,\phi) < 1$, all energy densities are present and are responsible for affecting the gravitational pull on any object. Thus, it is the gravitation affected by energy densities $\Omega_{\alpha e} + \Omega_{\alpha m,0}$, i.e., $X^2 + 2X(1-X)$, emergent from α, cumulatively with the gravitation affected by the baryonic energy density $\Omega_{bm,0}$, i.e., $(1-X)^2$, that determines galaxy rotational curves, gravitational lensing due to galaxies and galaxy clusters, velocity dispersion in galaxy clusters, galaxy formation, etc. Accordingly, *dark matter emerges from α, and, thus, is another manifestation of covarying coupling constants.* However, all of these energy densities are relative to the standard critical density ($\varepsilon^S_{c,0} \equiv 3c_0^2H_0^2/8\pi G_0$), rather than the critical density defined in the CCCs model ($\varepsilon^C_{c,0} \equiv 3c_0^2(H_0+\alpha)^2/8\pi G_0 = (1-X)^2\varepsilon^S_{c,0}$). Thus, in order to convert relative densities to physical densities in the CCCs model, we need to multiply them with $(1-X)^2$.

The question of how we determine $\Omega^S_{bm,0} \equiv (1-X)^2$, $\Omega^S_{\alpha e} \equiv X^2$, and $\Omega^S_{\alpha m,0} \equiv 2X(1-X)$ may arise. Since $X(r,\theta,\phi)$, all of the densities are $\Omega^S_{bm,0}(r,\theta,\phi)$, $\Omega^S_{\alpha e}(r,\theta,\phi)$, and $\Omega^S_{\alpha m,0}(r,\theta,\phi)$. However, we do not need to determine them explicitly as they are all expressed as functions of $X(r,\theta,\phi)$. The subscript 0 refers to the current time, rather than their fixed value in the cosmological sense.

Although the CCCs framework used in this work is phenomenological, its conceptual basis is not without theoretical support. A scalar–tensor action that generates a dynamical relationship between the speed of light $c(t)$ and the gravitational constant $G(t)$ was explicitly constructed and analyzed in our previous work [54]. In that formulation, the correlated variation in coupling constants arises naturally from the structure of the action and its field equations, providing a rigorous foundation for the interdependence assumed in the present CCCs cosmology. The current paper focuses on the observational and phenomenological consequences of this framework.

The tired light effect: The tired light (TL) model aligns closely with size data for high-redshift galaxies, particularly those imaged by the James Webb Space Telescope (JWST) [90]. This approach posits that photon energy loss, $h d\nu$, is proportional to the energy $h\nu$ and the path length dr, written as $d\nu = K\nu dr$, where K is the proportionality constant. Consequently, the proper distance d_p photons travel is derived easily as follows:

$$\frac{d\nu}{\nu} = Kdr \Rightarrow \int_{\nu_e}^{\nu_0}\frac{d\nu}{\nu} = K\int_{d_p}^{0} dr \Rightarrow \ln\left(\frac{\nu_0}{\nu_e}\right) = -Kd_p \Rightarrow \ln\left(\frac{\lambda_0}{\lambda_e}\right) = Kd_p. \tag{15}$$

Here, emitted and observed photon frequencies are ν_e and ν_0 and the respective wavelengths are λ_e and λ_0. By definition, the redshift is $z = (\lambda_0 - \lambda_e)/\lambda_e$, leading to $(1+z) = \lambda_0/\lambda_e$. Thus, tired light yields

$$d_p = \frac{1}{K}\ln(1+z). \tag{16}$$

This must reduce to Hubble's law $d_p = cz/H_0 = R_H z$ ($R_H = c/H_0$ being the Hubble radius) in the limit of $z \ll 1$, yielding $K = H_0/c = 1/R_H$. Thus, the proper distance in the tired light (TL) model is given by

$$d_p = \frac{c}{H_0}\ln(1+z). \tag{17}$$

One may be concerned about the use of the same value of the speed of light in the above expressions for all redshift values, where, in fact, it should be evolutionary, i.e., z-dependent. However, when one considers that the measurement unit of distance is also evolutionary, the two variations cancel out. Therefore, we can use the current value of c for all z values. This does not apply when only c or distance is involved, such as in determining the time dilation effect below, in the paragraph above Equation (22).

We can also write the expression for the proper distance in the CCCs model as follows [8]:

$$d_p = c\int_0^z \frac{dz}{H} = c\int_0^z \frac{dz}{(H_0+\alpha)(1+z)^{(3/2)}f(z)^{-(1/2)} - \alpha}. \tag{18}$$

Since photons travel distance d_p in an expanding universe and become 'tired' in doing so, the two proper distances must be the same, i.e.,

$$\frac{c}{H_t}\ln(1+z_t) = c\int_0^{z_x} \frac{dz}{(H_x+\alpha)(1+z)^{(3/2)}f(z)^{-(1/2)} - \alpha}. \tag{19}$$

Here, we have used subscript t to indicate tired light and x to label expanding universe-related quantities. Since both the expressions must reduce to Hubble's law, $d_p = cz/H_0$, in the zero-redshift limit and since $(1+z) = (1+z_x)(1+z_t)$, it yields $H_0 = H_x + H_t$ and [8]

$$H_t = \frac{(H_x+\alpha)}{2}\left(3 + \frac{\alpha}{H_x}\right) \tag{20}$$

Using the dimensionless parameter $X \equiv -\alpha/H_x$ defined in Equation (14), we may write Equation (19)

$$\int_0^{z_x} \frac{dz}{(1-X)(1+z)^{(3/2)}f(z)^{-(1/2)} + X} = \left[\frac{(1-X)}{2}(3-X)\right]^{-1}\ln\left[\frac{1+z}{1+z_x}\right]. \tag{21}$$

Given the free parameter α_x, this equation establishes a relationship between z and z_x, and thus also with z_t, through $(1+z) = (1+z_x)(1+z_t)$. We can now use either the left-hand side or right-hand side of Equation (19) to determine d_p.

To calculate an object's luminosity distance d_L in the CCCs model (excluding tired light), we analyze the evolution of photon energy flux with redshift. The energy of individual photons is attenuated by a factor of $(1+z)$. Furthermore, time dilation increases the arrival interval between photons by an additional factor of $(1+z)$. If photons are emitted with a time separation of δt_e, they are separated in space by $\delta r_e = c_e \delta t_e$. At observation, this becomes $\delta r_0 = c_0 \delta t_e (1+z)$, resulting in an observed time interval of $\delta t_0 = c_0 \delta t_e (1+z)/c_0 = \delta t_e (1+z)$. Thus, the scaling of luminosity distance mirrors that of the ΛCDM model, $d_L = d_p(t_0)(1+z)$, preserving the standard form of the distance modulus μ :

$$\mu = 5\log_{10}\left(d_p/1\text{Mpc}\right) + 5\log_{10}(1+z) + 25. \tag{22}$$

When determining the luminosity distance for the hybrid CCC+TL model, only $(1+z_x)$ is involved in time dilation, not $(1+z_t)$. Thus, combined with the photon energy reduction by $(1+z_x)$, the photon flux is reduced by $(1+z_x)^2$ due to the expansion of the universe, but only by $(1+z_t)$ due to tired light photon energy reduction. Since the distance is inversely proportional to the inverse square-root of the flux, the luminosity distance in the hybrid model becomes $d_L = d_p(1+z_x)(1+z_t)^{1/2}$. Also, since $(1+z_t) = (1+z)/(1+z_x)$, the distance modulus for the CCC+TL model becomes

$$\mu = 5\log_{10}\left(d_p/1\text{Mpc}\right) + 2.5\log_{10}[(1+z)(1+z_x)] + 25. \tag{23}$$

A similar expression can also be obtained for other hybrid models involving tired light.

It is now straightforward to fit the supernovae type 1a Pantheon+ data [91,92] to determine H_x and X, the two free parameters, and also H_t from Equation (20) and $H_0 = H_x + H_t$. We find H_X is 82% of H_0 and $X = 0.8$ for the CCC+TL model (see Table 1 of [8]). Once we know X, we can calculate all of the energy density components individually as in Equations (9) and (10). It is valuable to see how the various energy densities evolve cosmologically with the redshift z. How the densities evolve with z is shown graphically in Figure 1.

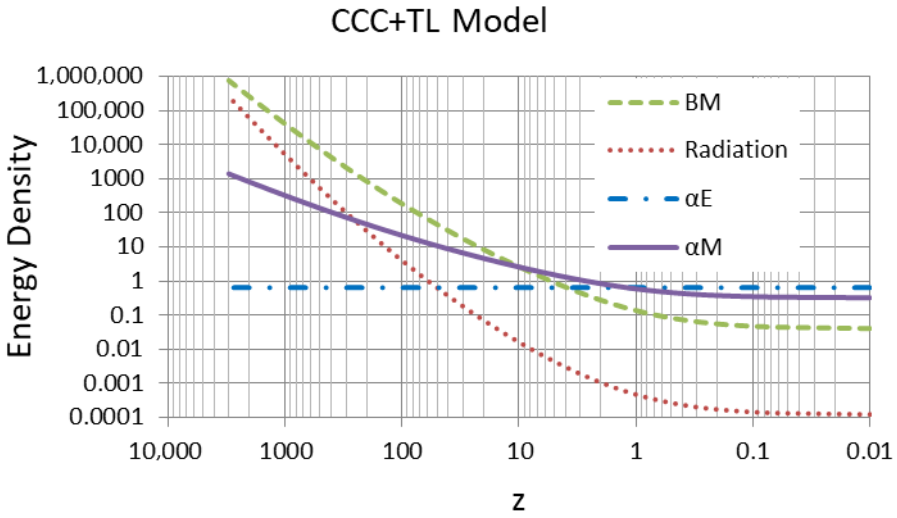

Figure 1. The evolution of various energy densities in the CCC+TL model plotted against the redshift (BM—baryonic matter, αE—α energy, and αM—α matter). (This figure is taken from [41]).

3. Cosmological Tests

The first test of any cosmological model is to see if it fits the supernovae type 1a standard candle data, such as Pantheon+ [91,92]. In Figure 2 we show the Pantheon+ data fit for four models: ΛCDM, ΛCDM + TL, CCCs, and CCC+TL. There is a visually indiscernible difference among the curves for the four models. The χ^2 values, too, are almost identical (see Table 1 in [8]). For the CCC+TL model, the parameters are $H_0 = 72.62$ km s^{-1}Mpc^{-1}, the CCC component of the Hubble constant $H_x = 0.82H_0$, $X = 0.80$. When using the CCC+TL model, we need to replace H_0 with H_x as required. Since $X = 0.8$, Equations (13) and (14) yield $\Omega_{bm,0} = 0.04$, $\Omega_{\alpha e} = 0.64$, and $\Omega_{\alpha m,0} = 0.32$. Each model has two free parameters (H_0 and $\Omega_{m,0}$ for ΛCDM, H_0 and X for CCCs, H_x and $\Omega_{m,0}$ for ΛCDM+TL, and H_x and X for CCC+TL) and they were determined by fitting the Pantheon+ data [91,92] in Gupta [8]. The critical density in the CCC+TL model relative to the ΛCDM model is $(H_x+\alpha)^2/H_0^2 = 0.027$, i.e., it comprises just the baryonic matter. It is worth reiterating that the inclusion of the tired light effect does not introduce an additional parameter since the relationship between the

expanding universe and the tired light parameters is determined by equating the expressions for the proper distance traveled by a photon in the two scenarios [8].

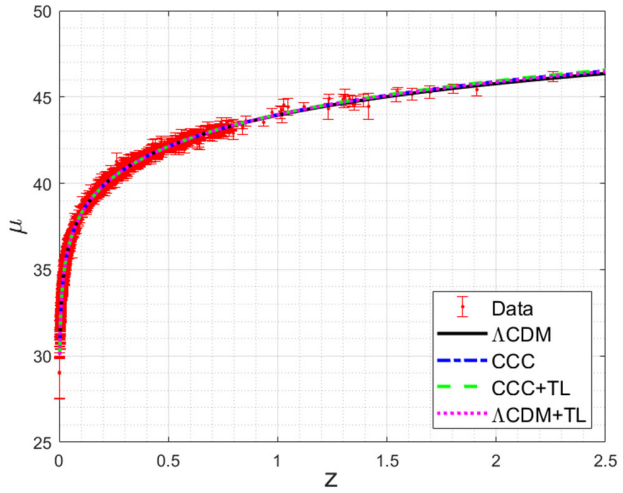

Figure 2. Pantheon+ [91,92] data fit for the four models discussed in the text. (This figure is taken from Gupta [8]).

Another test has become important during the James Webb Space Telescope (JWST) era, as JWST can see back in time to galaxies from the cosmic dawn, less than 0.3 Gyr after the Big Bang; galaxies at spectroscopically confirmed redshifts of greater than 14 have been observed. Surprisingly, their structure and masses appear to be as evolved as the galaxies in existence for over 10 Gyr, but they are too small in physical size, which is derived from their observed angular size calculated using the ΛCDM model (e.g., [18,93–105]). However, the physical sizes calculated using the CCC+TL model are more in-line with their expected size. Assuming galaxy sizes to be 10 kpc, in Figure 3 we show their expected angular size in different models as discussed above, as well as in the tired light model TL+ that includes a free parameter to better fit the Pantheon+ data (see [8] for details). For a galaxy to be 10 kpc in size, its angular size in the ΛCDM model has to be an order of magnitude larger than in the CCC+TL model, at $z \sim 10$.

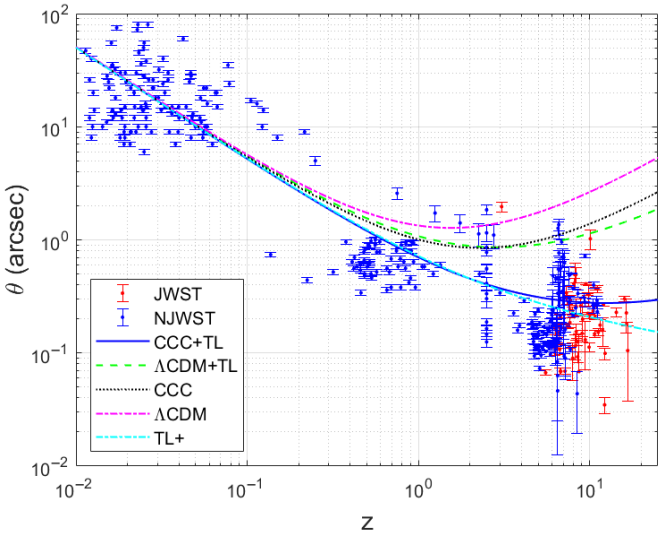

Figure 3. The angular size of 10 kpc objects for the five models, against the backdrop of measured angular sizes of galaxies from multiple sources, including the JWST data and some pre-JWST data labeled as NJWST (i.e., Not-JWST). (This figure is taken from [8]).

The literature extensively documents that galaxy sizes appear to decline with increasing redshift up to $z = 12.5$ (e.g., [106–111]). Figure 4, adapted from Gupta [112], displays these trends. While effective radius R_e curves are typically fitted with a power law of $(1+z)^s$, where $s = -1 \pm 0.3$, the CCC+TL model predicts a physical size increase following the inverse relation $R_e = (1+z)^{0.93}$. This intrinsic growth in the CCC+TL framework largely offsets the size reduction observed under ΛCDM assumptions, resulting in an effective evolution of $R_e \propto (1+z)^{s+0.93}$. For instance, the galaxy JADES-GS-z14-0 at $z = 14.18$ has a UV radius of $r_{uv} = 260 \pm 20$ pc in the ΛCDM model [105], but scales to 3172 ± 244 pc in the CCC+TL cosmology. The evolution, with redshift, of the mass, size, and density of galaxies and little red dots is the subject of a separate research paper [112].

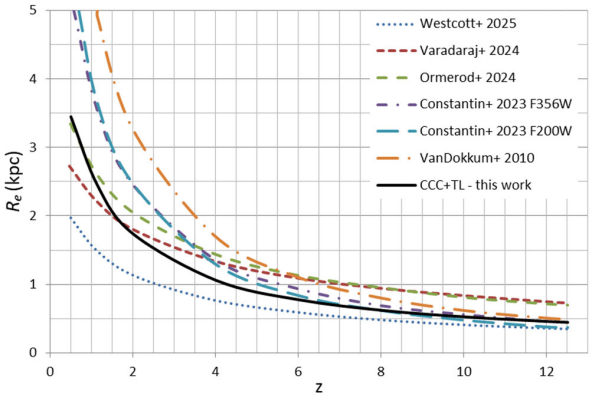

Figure 4. A comparison of the evolution of the effective radius R_e of galaxies with redshift z in different studies, as shown in the legend and discussed in the text. (This figure is taken from [112]).

Figure 5 illustrates the age advantage of the two hybrid models relative to the standard ΛCDM timeline. While both hybrids show an increase, the CCC+TL model provides a substantial 10-fold to 20-fold increase at redshifts 10 and 20, respectively. This corresponds to the available timeframes of 5.8 Gyr at $z = 10$ and 3.5 Gyr at $z = 20$, allowing ample time for the formation of massive galaxies. In comparison, the ΛCDM+TL model offers more modest age increases of 1.7 Gyr and 0.7 Gyr, respectively, [8] at the same redshifts. Thus, we may consider that the tired light effect is mainly responsible for increasing the universe's age, making it possible for massive galaxies to be observable at very high redshifts; the Capotauro object was detected tentatively at $z \sim 32$ and analyzed as most likely a massive galaxy [113]; such galaxies can easily fit within the CCC+TL cosmology once their redshifts are spectroscopically confirmed.

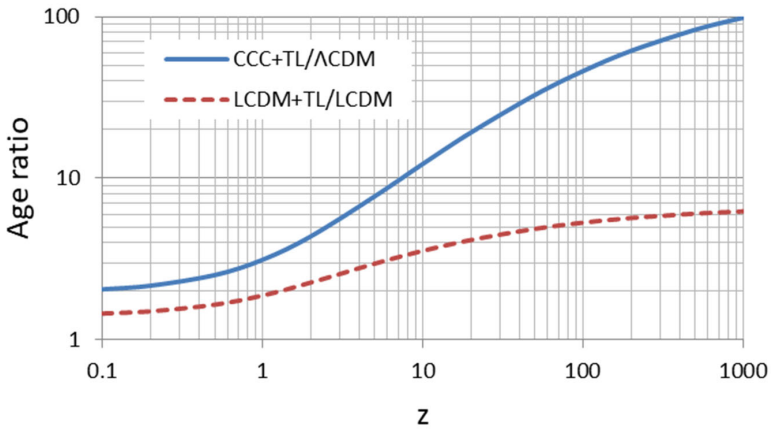

Figure 5. The age advantage of the two hybrid models over the ΛCDM model. (This figure is taken from [8]).

An essential test for a cosmological model is whether it can be fit to the cosmic microwave background (CMB) power spectrum. While our effort continues to fit the full Planck CMB power spectrum (Planck Collaboration [114]), we have been able to fit, with the CCC+TL model, the angular size of the sound horizon (first peak in the CMB power spectrum) and the corresponding baryon acoustic oscillation (BAO) data in the low redshift slices [40].

DESI (Dark Energy Spectroscopic Instrument) measurements have shown that dark energy is evolving. If we associate $\Omega_{\alpha e} + \Omega_{\alpha m}$ with dark energy with $\Omega_{\alpha e}$ as its static component and $\Omega_{\alpha m}$ as its dynamic component, we can see that it increases with the redshift at a rate similar to the recently reported observations up to the phantom crossing, when the equation of state parameter becomes less than -1 (DESI Collaboration: [115]), i.e., $f_{DE}(z) \equiv (\Omega_{\alpha e} + \Omega_{\alpha m}(z))/(\Omega_{\alpha e} + \Omega_{\alpha m,0}) = 1.17$ at $z = 0.5$ (Figure 1). The authors of the paper are not confident about the behavior of $f_{DE}(z)$ in their study beyond the phantom crossing ($z \sim 0.5$), which shows decreasing $f_{DE}(z)$ for $z > 0.5$. It should be mentioned that we have not used any free parameter to fit the DESI measurements; α is obtained by fitting Pantheon+ data.

We have shown that, despite the slower free-fall and cooling times, the formation of galaxies and other structures in the CCC+TL model without dark matter can happen very easily due to the model's age advantage and it starts happening at higher observed redshifts [41]. Nevertheless, proper galaxy formation modeling and simulation are required to strengthen these findings.

CCCs models do not suffer from the cosmological *coincidence problem* of the ΛCDM model that arises from the observation that dark matter and dark energy densities are comparable at the present time of human existence. Since the two evolve differently with redshift (i.e., time), it appears to be a coincidence that we are living in a very special epoch of cosmic evolution (e.g., [116]) when the two are about the same. Since dark matter and dark energy are absent in the native CCC+TL model, while α-energy and α-matter emerge from the single, non-evolving cosmological parameter α, there is no coincidence problem in CCCs models.

Objections raised against the tired light approach do not apply. We do not suggest that the tired light effect is caused by photons losing energy through Compton scattering. As the tired light component is relatively small, it does not interfere with the Tolman brightness test [117] due to the uncertainties in the brightness of the observed objects, nor with the time dilation test due to the large scatter in the time dilation data [41].

4. Astrophysical Tests

The most significant astrophysical evidence for the existence of dark matter is considered to be the observation of flat rotation curves in galaxies, as well as galaxy velocity dispersion in galaxy clusters and galaxies, large-scale structure formation, gravitational lensing, etc. We will see how CCCs models account for them. We will closely follow the treatment given by Gupta [118].

Galaxy rotation curves: Under the spherically symmetric galaxy approximation, for simplicity, the deemed observed mass $M_o(R)$ contributed by all the energy densities (not just by baryon energy density, as discussed above following Equation (14)) at a radius R is related to the Keplerian velocity $V_o(R)$ of a particle by (o-subscript, different from subscript 0, identifies quantities derived from observations),

$$\frac{GM_o(R)}{R} = V_o(R)^2; M_o(R) = 4\pi \int_0^R dr\rho(r)(1 - X(r))^2 r^2, \tag{24}$$

$$\frac{dM_o(R)}{R^2 dR} = 4\pi\rho(R)(1 - X(R))^2. \tag{25}$$

Why do we have $(1 - X(r))^2$ in the above equations? The contribution of all relative energy densities is 1 ($= (1 - X)^2 + X^2 + 2X(1 - X)$) from Equations (13) and (14) and it is $(1 - X)^2$, due to baryons. However, all of these energy densities are relative to the standard critical density ($\varepsilon^S_{c,0} \equiv 3c_0^2 H_0^2/8\pi G_0$) rather than the critical density defined in the CCCs model ($\varepsilon^C_{c,0} \equiv 3c_0^2(H_0 + \alpha)^2/8\pi G_0 = (1 - X)^2\varepsilon^S_{c,0}$). Thus, in order to convert relative densities to physical densities in the CCCs model, we need to multiply them with $(1 - X)^2$. Thus, total energy density is $\left((1 - X)^2 + X^2 + 2X(1 - X)\right) \times (1 - X)^2$, i.e., $(1 - X)^2$, and the baryon energy density is $(1 - X)^2 \times (1 - X)^2$, i.e., $(1 - X)^4$. Without the CCC correction, the integrand in Equation (24) would simply be $dr\rho(r)r^2$.

At a small R, matter density is very high, making the first term (baryon energy density) dominant, resulting in $X(R) = 0$. Thus, for low values of $R < R_t$, where R_t is defined below, we have

$$4\pi\rho_o(R \le R_t) = \frac{dM_o(R)}{R^2 dR} \tag{26}$$

This can be determined from observed galaxy rotation curves by numerical differentiation of V_o^2 vs. R data (Equations (24) and (25)). For $R > R_t$ (turn-off radius defined by Daod & Zeki 2019 [119]), the density variation is (since $X(R) \neq 0$):

$$4\pi\rho_o(R > R_t) = 4\pi\rho_o(R_t)(1 - X(R))^2 = \frac{dM_o(R)}{R^2 dR}. \tag{27}$$

Here, $4\pi\rho_o(R_t) = dM_o(R)/\left(R^2 dR\right)$ is determined at $R = R_t$. Having found $\rho_o(R_t)$ ($\equiv \rho_t$, the turn-off density), $X(R)$ can now be determined using Equation (27) by keeping ρ_t constant for $R > R_t$. With $X(R)$ known, we use Equations (24) and (25) in reverse, using numerical integration while replacing $(1 - X(r))^2$ with $(1 - X(r))^4$ to find the baryon mass M_{bX}(R) and the corresponding velocity curve $V_{bX}(R)$, comparing $V_{bX}(R)$ with $V_b(R)$, as determined by alternative methods represented in the SPARC database [120].

It should be mentioned that the SPARC data is provided for coarsely spaced radial values with significant uncertainties. This makes it difficult to reliably determine the density using Equation (27) since differentiation is sensitive to the data quality. Fortunately, numerical integration substantially alleviates this problem.

The question is, how do we determine R_t? It is not possible to apply the criterion Daod and Zeki [119] developed for the galaxy NGC3198 to most other galaxies. Additionally, since most SPARC data is for coarsely spaced radial values, it is not possible to select the value that might provide the best fit for a galaxy from the data points. A better approach is to use the density-based turn-off parameter ρ_t. It provides a more robust galaxy parameter than the turn-off radius and is possibly more relevant in our context.

Using the turn-off density criterion inspired by Daod and Zeki's [119] turn-off radius criterion, we analyzed the SPARC data for the galaxy NGC6503 as described above and obtained the curves depicted in Figure 6; it is one of several randomly selected galaxy rotation curves from the SPARC database fitted in the paper [118]. Considering that the baryon curve V_b from the SPARC database is an approximation based on multiple observations for the galaxy's bulge, gas, and disk, and our fit V_{bX} is ideal only for spherically symmetric galaxy morphologies, the two baryon curves can be considered comparable in shape and values.

The tabulated data in the SPARC database [120] needed correction for the mass-to-light ratios of galaxy disks and bulges. We have used nominal values of 0.5 for disks and 0.7 for bulges (McGaugh [121]) to correct the respective velocities in the SPARC database, which

uses a mass-to-light ratio of unity for both. Thus, we compute the baryon velocity, V_b, curves using $V_b = \left(V_{gas}^2 + 0.5V_{disc}^2 + 0.7V_{bul}^2\right)^{1/2}$.

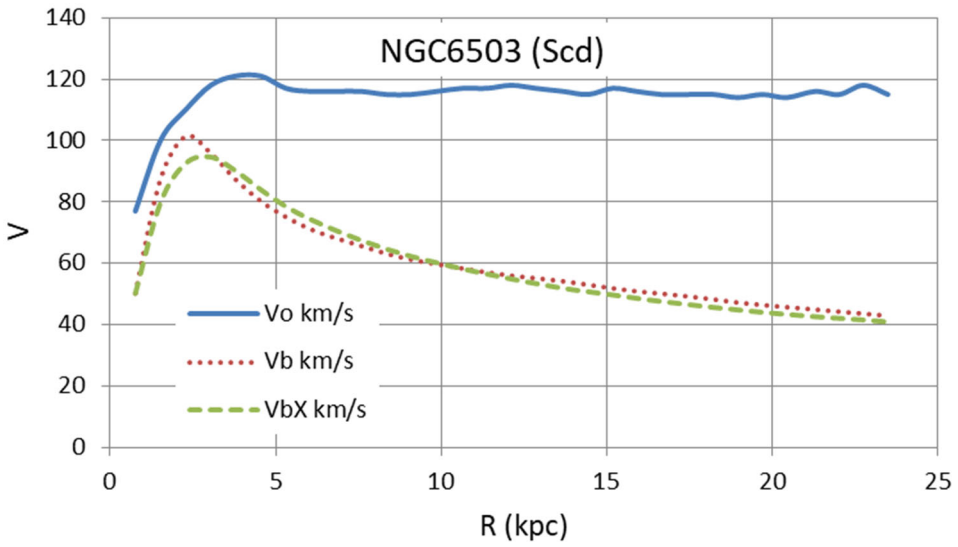

Figure 6. Galaxy rotation curves for NGC 6503 (Scd), with turn-off density given by $\rho_t = 5.17 \times 10^{-24}$ gcm^{-3}, giving the turn-off radius $R_t = 1.9$ kpc. Vo designates the observed rotational velocity curve and Vb denotes the baryon contribution to it, as per the SPARC. The Vbx label is for the derived baryon matter from the CCC+TL model. (This figure is taken from [118]).

We also tried to determine the scaling of densities ρ_o and ρ_{bX} with R, where the observed rotation curve $V_0(R)$ is flat, i.e., constant. Then, differentiating $GM_o(R)/R = V_o(R)^2$ from Equation (24), we get

$$\frac{GdM_o(R)}{RdR} - \frac{GM_o(R)}{R^2} = 0 \Rightarrow \frac{GdM_o(R)}{R^2dR} = \frac{GM_o(R)}{R}\left(\frac{1}{R^2}\right) = \frac{V_o(R)^2}{R^2}, \text{ or} \tag{28}$$

$$\frac{dM_o(R)}{R^2dR} \propto \frac{1}{R^2}. \tag{29}$$

Therefore, from Equation (27),

$$4\pi\rho_o(R) = 4\pi\rho(R_t)(1 - X(R))^2 = \frac{V_o(R)^2}{GR^2} \Rightarrow (1 - X(R))^2 \sim \frac{1}{R^2} \Rightarrow 1 - X(R) \sim R^{-1}, \tag{30}$$

we obtain $\rho_o(R) \sim 1/R^2$ beyond the turn-off radius when ρ is constant as ρ_t. Since $\rho_{bX} \sim (1 - X(R))^4$, we obtain $\rho_{bX} \sim 1/R^4$ for $R \gg R_t$, similar to Hernquist's [122] model, in which density falls as R^{-4} beyond a characteristic radius [123]. Recall that we have used spherical symmetry for galaxy morphology.

We noticed that, while the turn-off radius R_t spread is over a factor of about eight for the galaxies we studied, the turn-off density ρ_t spread is only over a factor of about four [118]. Thus, we consider the turn-off density to be a more robust fit parameter. The fact that these parameters vary from galaxy to galaxy is not surprising, considering our very simple approach that assumes spherical symmetry; galaxies are far from being spherically symmetric and exhibit different morphologies. It is worth mentioning that the turn-off acceleration $a_t \equiv V_{flat}^2/R_t$ turns out to be about the same order as the Milgromian (MOND) acceleration $a_0 = 1.2 \times 10^{-8}$cm s^{-2} [124].

Another factor that can affect the turn-off density is the size of a galaxy. For a given radial density profile, the projected density on the galactic plane is proportional to the galaxy size. Thus, we can expect the turn-off density estimated by fitting the data to be

inversely proportional to the galactic size for similar actual densities, especially when considering galaxies of vastly differing sizes, such as dwarf galaxies and ultra-faint dwarf galaxy satellites in the Milky Way.

Density distribution in galaxy clusters: Next, we considered the role of α-matter and α-energy in the galaxy clusters. To realistically estimate this, we should determine the mass density distribution around each galaxy at its location in the cluster and superimpose them for all the galaxies in a cluster. Nevertheless, we decided to treat a galaxy cluster similarly to a galaxy to determine its density profile and calculate its baryonic density curve to compare it with that in the original paper (Mandelbaum et al. [125], Figure 1). This is depicted in Figure 7 and shows a good visual fit when the turn-off density is set to $\rho_t = 2.0 \times 10^{-24}$ g cm^{-3}. This density turns out to be in the same range as the turn-off density for the galaxies we studied.

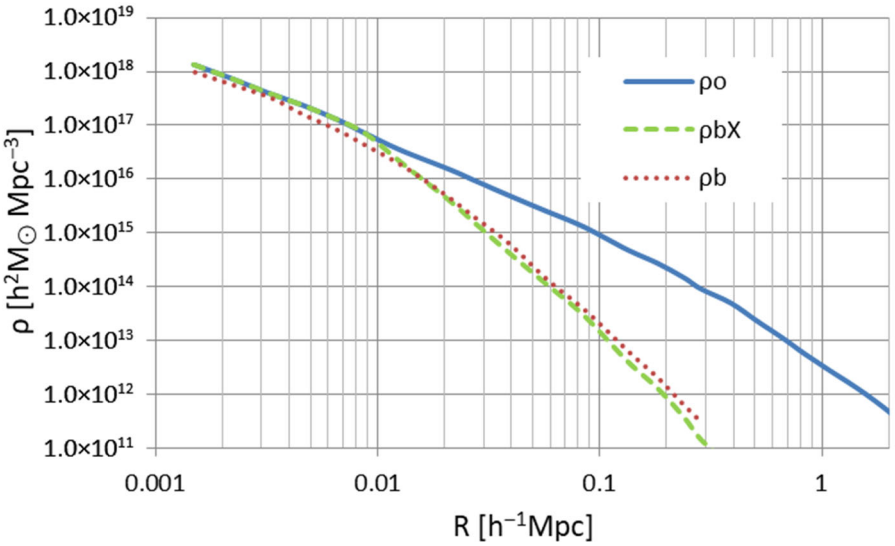

Figure 7. Density profile ρ(R) for a typical galaxy cluster. The total density profile ρ_o (blue line) and baryonic density profile ρ_b (red dotted line) are from Mandelbaum et al. (2006) [125]. The reduced Hubble constant is $h = \mathrm{H}_0/(100 \text{ km s}^{-1} \text{ Mpc}^{-1})$. The density ρ_{bX} is calculated using a ρ_o similar to our calculations for galaxy rotation curves with $\rho_t = 5.74 \times 10^{16}\, h^2 \mathrm{M}_\odot \mathrm{Mpc}^{-3} = 2.0 \times 10^{-24}$ g cm^{-3} (assuming $h = 0.72$ for the standard cosmology). (This figure is taken from [118]).

Gravitational lensing is a vast field to consider in this multifaceted work. So, we will consider it very briefly, in principle, and see how we can explain the gravitational lensing by the JWST-ER1 galaxy of background objects, following van Dokkum et al. [126] and Kong et al. [127]. Kong et al. [127] used a Hernquist density profile $\rho_b(r)$ to model the radial stellar distribution [122,128] as given by

$$\rho_b(r) = \frac{M_b}{2\pi} \frac{r_a}{r} \frac{1}{(r_a + r)^3}. \tag{31}$$

Here, M_b is the total stellar mass and r_a is the characteristic radius. The parameters for JWST-ER1 are taken as follows [126,127]: $M_b = 1.3 \times 10^{11} M_\odot$, $r_a = 0.79$ kpc, the Einstein ring $R_E = 6.6$ kpc, the total mass within the Einstein ring $M_E = 6.5 \times 10^{11} M_\odot$, and the redshift $z \approx 2$. As discussed above for the galaxy rotation curves, the turn-off density and turn-off radius play critical roles in achieving a good fit to the observations. As shown in Figure 1, one would expect them to be significantly modified compared to the values for $z = 0$. Also, the size, mass, and density values are affected as discussed in the context of Figure 4. Nevertheless, we will try to determine the lensing parameter with the initial

assumption that the galaxy is at $z = 0$. We will then discuss how they are affected due to the galaxy being at $z \neq 0$.

Assuming the turn-off radius $R_t = r_a$, we obtain, for the stellar mass M_b,

$$\rho_t(r = R_t = r_a) = \frac{M_b}{16\pi r_a^3}. \tag{32}$$

Let us assume, incorrectly, that the stellar mass comprises the total baryon mass. Accordingly, for baryons,

$$\rho_b(r \geq r_a) = \rho_t(1 + X(r))^4 = \frac{M_b}{2\pi}\frac{r_a}{r}\frac{1}{(r_a + r)^3} \Rightarrow (1 + X(r))^4 = 8\left[\frac{r}{r_a}\left(1 + \frac{r}{r_a}\right)^3\right]^{-1} \text{ for } r \geq r_a. \tag{33}$$

Thus, for the observed gravitational lensing effect, the apparent density is

$$\rho_o(r \geq r_a) = \rho_t(1 + X(r))^2 = 2.828\rho_t\left[\frac{r}{r_a}\left(1 + \frac{r}{r_a}\right)^3\right]^{-1/2} \text{ for } r \geq r_a. \tag{34}$$

The mass for $r \leq r_a$ is the same for the two cases, as it is just the baryon mass fraction within r_a,

$$M_b(r \leq r_a) = 4\pi\int_0^{r_a}\frac{M_b}{2\pi}\frac{r_a}{r}\frac{r^2 dr}{(r_a + r)^3} = 2M_b\int_0^{r_a}\frac{r_a r dr}{(r_a + r)^3} = 2M_b \times \frac{1}{8} = \frac{M_b}{4}. \tag{35}$$

The total baryon mass within the Einstein ring R_E is,

$$M_b(0 \leq r \leq R_e) = 4\pi\int_0^{R_E}\frac{M_b}{2\pi}\frac{r_a}{r}\frac{r^2 dr}{(r_a + r)^3} = M_b\left(1 + \frac{r_a}{R_E}\right)^{-2} = 0.80M_b = 1.04 \times 10^{11}M_\odot. \tag{36}$$

The apparent total mass for $r_a \leq r \leq R_E$ with $r_a = 0.79$ kpc and $R_E = 6.6$ kpc

$$M_o(r_a \leq r \leq R_E) = 4\pi\int_{r_a}^{R_E}\rho_o(r)r^2 dr = \frac{0.707M_b}{r_a^3}\int_{r_a}^{R_E}\left[\frac{r}{r_a}\left(1 + \frac{r}{r_a}\right)^3\right]^{-1/2} r^2 dr = 3.67M_b. \tag{37}$$

This yields $M_o(0 \leq r \leq R_e) = (3.67 + 0.25)M_b = 3.92M_b = 4.1 \times 10^{11}M_\odot$. Considering the crude assumptions we have made, it is not too different from the observed value of $6.5 \times 10^{11}M_\odot$. Since stellar mass is one component of the baryonic mass, the discrepancy could partially result from this difference between the stellar mass and the total baryonic mass. An additional discrepancy could be due to the spherically symmetric assumption used in deriving our equations. Also, the use of Hernquist density profile $\rho_b(r)$ to model the radial stellar distribution [122,128] has its own limitations. Thus, we could say that our approach is consistent with the gravitational lensing observations.

Since the JWST-ER1 galaxy is at $z = 2$, we need to consider how it affects the various galaxy parameters in the CCC+TL model relative to the ΛCDM model. The size and dynamical mass of the galaxy increases by 2.8 and the stellar mass by 1.15 [112], whereas the volumetric density decreases to about 4%. Thus, the turn-off density ρ_t $\left(352 \times 10^{-24}\text{g cm}^{-3}\right)$ calculated above at $z = 0$ decreases to $14 \times 10^{-24}\text{g cm}^{-3}$, closer to the value for the galaxy rotation curves and galaxy clusters. It is not a bad estimate considering that the Hernquist baryon density profile [122] has its limitations, and does not represent the true baryon density profile in a galaxy. In addition, various densities are affected as per Equation (10). These changes will, in turn, affect the lensing parameters and observational outcome. We expect to consider this in a separate paper.

Ultra-faint dwarf galaxies: We will now consider an ultra-faint dwarf galaxy, Reticulum II, which is considered to be mostly dark matter in the standard cosmology

(e.g., [129–131]). This galaxy has the following parameters that are of interest to us [130]: $M_{dyn} = 5.6 \pm 2.4 \times 10^5 M_\odot$ (using dispersion velocity $\sigma = 3.3 \pm 0.7$ km s^{-1}); the half-light radius $r_{1/2} = 55 \pm 5$ pc; and the mass-to-light ratio $M/L_V = 470 \pm 210$. Taking $M_*/L_V = 2$, we find the stellar (baryonic) mass $M_* \equiv M_b \approx 2.4 \times 10^3 M_\odot$. Taking the same $\rho_t = 5.17 \times 10^{-24}$ g cm^{-3} as in Figure 6 for NGC 6503, that has $R_{eff} \equiv r_{1/2} = 1.62$ kpc [118], the turn-off density for Reticulum II needs to be scaled to $\rho_t = 5.17 \times 10^{-24}$ g cm^{-3} $\times\, 1620/55 = 152 \times 10^{-24}$ g cm^{-3} (as discussed above at the end of subsection '*Galaxy rotation curves*'. From Equation (32),

$$\rho_t(r = r_a) = \frac{M_b}{16\pi r_a^3} = 1.52 \times 10^{-22} \text{ g cm}^{-3}. \tag{38}$$

This gives $r_a = 1.28$ pc. Using Equation (32), we may write

$$M_o(r_a \le r \le r_{1/2}) = \frac{0.707 M_b}{r_a^3} \int_{r_a}^{r_{1/2}} \left[\frac{r}{r_a} \left(1 + \frac{r}{r_a} \right)^3 \right]^{-1/2} r^2 dr = 26.5 M_b. \tag{39}$$

The contribution from $r \le r_a$ (Equation (35)), $0.25 M_b$, is negligible in comparison. We thus see that Reticulum II has very little baryonic mass using the dynamical mass measurement, and the latter can result from the CCCs effect rather than from dark matter. Considering the considerable uncertainty in the observed numbers and our crude estimation, it is heartening to see that the CCCs approach is not inconsistent with the observations.

We can apply a similar approach to understand the galaxies classified as dark matter-deficient. For example, NGC 1277, designated as dark matter-deficient (e.g., [132]), will have its turn-off density at a larger radius than standard galaxies. It will result in the dark matter equivalent of the CCCs effect, appearing at higher radii than normal and thus will appear to be dark matter-deficient.

We have also discussed the preliminary galaxy formation test in the CCC+TL cosmology under the Cosmological Test section above. Due to the age advantage of this model, galaxy formation without dark matter can proceed normally—there is no need for extreme mass accumulation conditions in the dark ages [41]. However, we have yet to do a galaxy formation simulation using this approach.

Many more tests can be conducted using the approach outlined here and its subsequent improvements.

5. Discussion

The primary objective of this paper is to explore whether dark matter and dark energy are physical entities or if they are manifestations of some cosmological effect that is not detectable in the local universe with our existing capabilities. Lots of effort and resources have been allocated to studies that assume their physical existence, as derived from the Friedmann equations of the ΛCDM model. The cosmological constant Λ is thought to give rise to dark physical energy, exerting a repulsive force, while the matter term is significantly larger than the observable mass of the universe, leading to the belief that this difference constitutes dark physical matter. However, the Friedmann equations do not specify what constitutes the various terms in them. That is why one looks for evidence of dark matter and dark energy in astrophysical and cosmological observations, as well as in laboratories such as the Large Hadron Collider. The Friedmann equations do not specify how normal matter, dark matter, and dark energy are distributed throughout the universe. One has to make assumptions and apply other physical laws to explain the formation of stars, black holes, galaxies, large-scale structures, etc., and to explain observations such as galaxy rotation curves, velocity dispersion in galaxies and galaxy clusters, and gravitational lensing.

We have shown that if we generalize Dirac's idea of an evolving gravitational constant to all coupling constants and connect their variations through a dimensionless function $f(t)$ derived from the local energy conservation expression, we obtain Friedmann equations that reproduce the dark matter- and dark energy-type terms of the ΛCDM model in terms of the constant that defines the time variation in the function. Effectively, we introduced the variation in a constant proportional to its length dimensionality, e.g., G has length dimensionality L^3, so $G \sim f(t)^3$. The same is applied to any variable containing length, e.g., distance, velocity, and acceleration. Thus, $f(t) \rightarrow f(z)$ serves as another scale factor that affects the length dimension itself.

Dark matter and dark energy do not exist in the native Friedmann equations (Equations (2)–(4)) in the CCC models. They only contain the CCC parameter α. Only when we expand Equation (2) and compare it with a similar equation for the ΛCDM model are we able to relate some terms in the CCC equations with the dark energy and dark matter in the ΛCDM model. It means that the dark matter and dark energy terms of the ΛCDM model emerge from the variation in coupling constants. It is thus prudent to suggest that dark matter and dark energy are not physical and do not contribute to the energy content of the universe, i.e., that the energy content of the universe comprises baryonic matter and radiation. The dark energy and dark matter values have not been measured astrophysically, only predicted by the ΛCDM cosmology.

The CCC parameter α that determines the variation in constants has a constant cosmological value, which is involved in the critical density and thus in the cosmological normal matter density. Just as the normal matter density can vary locally, i.e., astrophysically, so α can also vary locally within its permitted limits of $-H_0 < \alpha < 0$ in response to the matter density changes under gravitational pull to form astrophysical structures. Now, from Equations (13) and (14), high baryon local density (such as in the solar system) means $\alpha = 0$, i.e., all the constants have fixed values as we know them from our measurements. However, as the baryon density falls with the galaxy radius and reaches a point (the turn-off point), α starts to decrease and α-energy and α-matter terms become effective. These terms then cumulatively affect the galaxy rotation curves similarly to the dark matter of the ΛCDM model. They play a similar role in galaxy cluster dynamics. They are involved in other astrophysical observations attributed to dark matter, such as gravitational lensing, dark matter-dominant and dark matter-deficient galaxies, ranging from ultra-faint dwarfs to massive galaxies.

The CCCs model, when fitted to the Pantheon+ data, yields $\alpha = -0.5H_0$ (Gupta 2023 [8]) and fits the data as well as the ΛCDM model (Figure 2). However, it does not fit well the James Webb observations of the small angular sizes of galaxies at high redshifts (Figure 3). When we allow the tired light (TL) effect of Zwicky [1,133] to coexist with the expanding CCCs universe and call it the CCC+TL model, we find a good fit as shown in Figure 3. We have found that the CCC+TL model provides better consistency with observational data in all our studies. The Friedmann equations of the CCCs models are consistent with both cosmological and astrophysical observations without the need for additional physics; for example, Equation (14) is an expression of the first Friedmann equation used to fit galaxy rotation curves. All other models, including ΛCDM and MOND, do not use the Friedmann equations to explain astrophysical observations.

Tired light limitations that led to the rejection of this concept, such as Compton scattering, time dilation, the Tolman brightness test, and the CMB isotropy, do not apply, as discussed in earlier papers (e.g., Gupta [40,41,112,118]), primarily because the tired light effect exists in parallel with the universe's expansion.

Since the CCC+TL model is founded on the extension of the ideas of Dirac and Zwicky, we could consider this model to belong to the Dirac–Zwicky cosmology.

6. Conclusions

- Dark matter and dark energy are manifestations of the interrelated variation in coupling constants (covarying coupling constants or CCC) over cosmic time; they emerge from this variation and create the illusion of dark energy and dark matter. They have no physical existence.
- The CCCs cosmology is astrophysically and cosmologically consistent and does not require new physics to connect with their respective observations.
- Dark matter and dark energy have the same origin—the CCC parameter α.
- The CCCs cosmology does not suffer from the coincidence problem.
- The CCCs cosmology is consistent with DESI observations of dark energy increasing with redshift up to the phantom crossing.
- Substantial work is required to establish whether the CCC+TL model offers an extension of ΛCDM cosmology and reduces observed cosmological and astrophysical tensions.

Funding: This research received no external funding.

Data Availability Statement: Citations have been provided for the data used in this work.

Acknowledgments: The author is grateful to Rodrigo Cuzinatto, Utkarsh Kumar, Pedro Pompeia, and Piyush Singhal for providing helpful discussions. He wishes to express his most sincere thanks to the four reviewers and the academic editor of the paper, their critical constructive comments helped reshape this paper significantly.

Conflicts of Interest: The authors declare no conflict of interest.

References

1. Zwicky, F. Die Rotverschiebung von extragalaktischen Nebeln [The red shift of extragalactic neubulae]. *Helv. Phys. Acta* **1933**, *6*, 110–127. (In Germany)
2. Rubin, V.C.; Ford, W.K., Jr. Rotation of the Andromeda Nebula from a Spectroscopic Survey of Emission Regions. *Astrophys. J.* **1970**, *150*, 379. [CrossRef]
3. Rubin, V.C.; Ford, W.K., Jr.; Thonnard, N. Extended rotation curves of high-luminosity spiral galaxies. IV. Systematic dynamical properties, SA through SC. *Astrophys. J.* **1978**, *225*, L107–L111. [CrossRef]
4. Einstein, A. Kosmologische Betrachtungen zur allgemeinen Relativitätstheorie. In *Das Relativitätsprinzip: Eine Sammlung von Abhandlungen*; Vieweg+ Teubner Verlag: Wiesbaden, Germany, 1917; pp. 142–152.
5. Riess, A.G.; Filippenko, A.V.; Challis, P.; Clocchiatti, A.; Diercks, A.; Garnavich, P.M.; Gilliland, R.L.; Hogan, C.J.; Jha, S.; Kirshner, R.P.; et al. Observational Evidence from Supernovae for an Accelerating Universe and a Cosmological Constant. *Astron. J.* **1998**, *116*, 1009–1038. [CrossRef]
6. Perlmutter, S.; Aldering, G.; Goldhaber, G.; Knop, R.A.; Nugent, P.; Castro, P.G.; Deustua, S.; Fabbro, S.; Goobar, A.; Groom, D.E.; et al. Measurements of Ω and Λ from 42 High-Redshift Supernovae. *Astrophys. J.* **1999**, *517*, 565–586. [CrossRef]
7. Milgrom, M. A modification of the Newtonian dynamics as a possible alternative to the hidden mass hypothesis. *Astrophys. J.* **1983**, *270*, 365–370. [CrossRef]
8. Gupta, R.P. JWST early Universe observations and ΛCDM cosmology. *Mon. Not. R. Astron. Soc.* **2023**, *524*, 3385–3395. [CrossRef]
9. Desmond, H. Modified Newtonian Dynamics: Observational Successes and Failures. *arXiv* **2025**, arXiv:2505.21638. [CrossRef]
10. Kroupa, P.; Pawlowski, M.; Milgrom, M. The failures of the standard model of cosmology require a new paradigm. *Int. J. Mod. Phys. D* **2012**, *21*, 1230003. [CrossRef]
11. Capozziello, S.; De Laurentis, M. The dark matter problem from f(R) gravity viewpoint. *Ann. Phys.* **2012**, *524*, 545. [CrossRef]
12. Farnes, J.S. A unifying theory of dark energy and dark matter: Negative masses and matter creation within a modified ΛCDM framework. *Astron. Astrophys.* **2018**, *620*, A92. [CrossRef]
13. Verlinde, E.P. On the origin of gravity and the laws of Newton. *J. High Energy Phys.* **2011**, *1104*, 029. [CrossRef]
14. Gonzalo, E.; Montero, M.; Obied, G.; Vafa, C. Dark Dimension Gravitons as Dark Matter. *arXiv* **2022**, arXiv:2209.09249. [CrossRef]
15. Yahalom, A. The Geometrical Meaning of Time. *Found. Phys.* **2008**, *38*, 489–497. [CrossRef]
16. Wagman, M.; Horwitz, L.P.; Yahalom, A. Applying Retardation Theory to Galaxies. *J. Phys. Conf. Ser.* **2023**, *2482*, 012005. [CrossRef]

17. Mannheim, P.D. Alternatives to dark matter and dark energy. *Prog. Part. Nucl. Phys.* **2006**, *56*, 340–445. [CrossRef]
18. Austin, D.; Adams, N.J.; Conselice, C.J.; Harvey, T.; Ormerod, K.; Trussler, J.; Li, Q.; Ferreira, L.; Dayal, P. The evolution of the galaxy stellar mass function at $3.5 \leq z \leq 7.5$ from a large sample of Lyman-break galaxies in the JWST CEERS survey. *arXiv* **2023**, arXiv:2302.04270.
19. Skordis, C.; Złośnik, T. New Relativistic Theory for Modified Newtonian Dynamics. *Phys. Rev. Lett.* **2021**, *127*, 161302. [CrossRef]
20. Roberts, M.G.; Kapalinghat, M.; Valli, M.; Yu, H.-B. Gravothermal collapse and the diversity of galactic rotation curves. *arXiv* **2024**, arXiv:2407.15005. [CrossRef]
21. Mistele, T.; McGaugh, S.; Lelli, F.; Schombert, J.; Li, P. Indefinitely Flat Circular Velocities and the Baryonic Tully–Fisher Relation from Weak Lensing. *Astrophys. J. Lett.* **2024**, *969*, L3. [CrossRef]
22. Brouwer, M.M.; Oman, K.A.; Valentijn, E.A.; Bilicki, M.; Heymans, C.; Hoekstra, H.; Napolitano, N.R.; Roy, N.; Tortora, C.; Wright, A.H.; et al. The weak lensing radial acceleration relation: Constraining modified gravity and cold dark matter theories with KiDS-1000. *Astron. Astrophys.* **2021**, *650*, A113. [CrossRef]
23. Hoeneisen, B. Why do galaxies have extended flat rotation curves? *Int. J. Astron. Astrophys.* **2025**, *15*, 1–10. [CrossRef]
24. Buzzo, M.L.; Forbes, D.A.; Romanowski, A.J.; Haacke, L.; Gannon, J.S.; Tang, Y.; Hilker, M.; Ferré-Mateu, A.; Janssens, S.R.; Brodi, J.P.; et al. A new class of dark matter-free dwarf galaxies? I. Clues from FCC 224, NGC 1052-DF2 and NGC 1052-DF4. *arXiv* **2025**, arXiv:2502.05405. [CrossRef]
25. Jovanovic, V.B.; Capozziello, S.; Jovanovic, P.; Borka, D. Recovering the fundamental plane of galaxies by f(R) gravity. *arXiv* **2016**, arXiv:1610.03336. [CrossRef]
26. Jovanovic, V.B.; Borka, D.; Jovanovic, P. The baryonic Tully-Fisher relation and Fundamental Plane in the light of f(R) gravity. *arXiv* **2025**, arXiv:2504.11135.
27. Di Valentino, E.; Said, J.L.; Riess, A.; Pollo, A.; Poulin, V.; Gómez-Valent, A.; Weltman, A.; Palmese, A.; Huang, C.D.; van de Bruck, C.; et al. The CosmoVerse White Paper: Addressing observational tensions in cosmology with systematics and fundamental physics. *arXiv* **2025**, arXiv:2504.01669. [CrossRef]
28. Sami, M.; Myrzakulov, R. Late time cosmic acceleration: ABCD of dark energy and modified theories of gravity. *Int. J. Mod. Phys. D* **2015**, *25*, 1630031. [CrossRef]
29. Austin, J.; Jain, B.; Khoury, J.; Trodden, M. Beyond the cosmological standard model. *Phys. Rep.* **2015**, *568*, 1–98. [CrossRef]
30. Lombriser, L.; Lima, N. Challenges to Self-Acceleration in Modified Gravity from Gravitational Waves and Large-Scale Structure. *Phys. Letts. B* **2017**, *765*, 382–385. [CrossRef]
31. Shankaranarayanan, S.; Johnson, J.P. Modified theories of gravity: Why, how and what? *Gen. Relativ. Gravit.* **2022**, *54*, 44. [CrossRef]
32. Faraoni, V.; Jacques, A. Cosmological expansion and local physics. *Phys. Rev. D* **2007**, *76*, 063510. [CrossRef]
33. Guariento, D.C.; Fontanini, M.; da Silva, A.M.; Abdalla, E. Realistic fluids as source for dynamically accreting black holes in a cosmological background. *Phys. Rev. D* **2012**, *86*, 124020. [CrossRef]
34. Maciel, A.; Guariento, D.C.; Molina, C. Cosmological black holes and white holes with time-dependent mass. *Phys. Rev. D* **2015**, *91*, 084043. [CrossRef]
35. Croker, K.S.; Weiner, J.L. Implications of Symmetry and Pressure in Friedmann Cosmology. *I. Formalism. Astrophys. J.* **2019**, *882*, 19. [CrossRef]
36. Farrah, D.; Petty, S.; Croker, K.S.; Tarlé, G.; Zevin, M.; Hatziminaoglou, E.; Shankar, F.; Wang, L.; Clements, D.L.; Efstathiou, A.; et al. A Preferential Growth Channel for Supermassive Black Holes in Elliptical Galaxies at $z \lesssim 2$. *Astrophys. J.* **2023**, *943*, 133. [CrossRef]
37. Ghodla, S.; Easther, R.; Briel, M.M.; Eldridge, J.J. Observational implications of cosmologically coupled black holes. *arXiv* **2023**, arXiv:2306.08199. [CrossRef]
38. Berglund, P.; Hübsch, T.; Minić, D. Dark energy and string theory. *Phys. Letts. B* **2019**, *798*, 134950. [CrossRef]
39. McDonough, E.; Scalisi, M. Towards Early Dark Energy in String Theory. *arXiv* **2022**, arXiv:2209.00011. [CrossRef]
40. Gupta, R.P. Testing CCC+TL Cosmology with Observed Baryon Acoustic Oscillation Features. *Astrophys. J.* **2024**, *964*, 55. [CrossRef]
41. Gupta, R.P. On Dark Matter and Dark Energy in CCC+TL Cosmology. *Universe* **2024**, *10*, 266. [CrossRef]
42. Gilbert, C. Dirac's cosmology and the general theory of relativity. *Mon. Not. R. Astron. Soc.* **1956**, *116*, 684. [CrossRef]
43. Gilbert, C. Dirac's Cosmology. *Nature* **1961**, *192*, 57. [CrossRef]
44. Canuto, V.; Londenquai, J. Dirac cosmology. *Astrophys. J.* **1977**, *211*, 342–356. [CrossRef]
45. Dirac, P.A.M. The Cosmological Constants. *Nature* **1937**, *139*, 323. [CrossRef]
46. Gupta, R.P. Varying coupling constants and their interdependence. *Mod. Phys. Lett. A* **2022**, *37*, 23. [CrossRef]
47. Uzan, J.-P. Varying Constants, Gravitation and Cosmology. *Living Rev. Relativ.* **2011**, *14*, 2. [CrossRef] [PubMed]
48. Maeder, A.; Gueorguiev, G.V. The growth of the density fluctuations in the scale-invariant vacuum theory. *Phys. Dark Universe* **2019**, *25*, 100315. [CrossRef]

49. Maeder, A.; Gueorguiev, G.V. The Scale-Invariant Vacuum (SIV) Theory: A Possible Origin of Dark Matter and Dark Energy. *Universe* **2020**, *6*, 46. [CrossRef]
50. Maeder, A. An alternative to the λcdm model: The case of scale invariance. *Astrophys. J.* **2017**, *834*, 194. [CrossRef]
51. Brans, C.; Dicke, R.H. Mach's principle and a relativistic theory of gravitation. *Phys. Rev.* **1961**, *124*, 925. [CrossRef]
52. Weyl, H. Gravitation and electricity Sitzungsber. *Preuss. Akad. Wiss.* **1918**, 465–480.
53. Romero, C.; Fonseca-Neto, J.C.; Pucheu, M.L. General relativity and Weyl geometry. *Class. Quantum Gravity* **2012**, *29*, 155015. [CrossRef]
54. Cuzinatto, R.R.; Gupta, R.P.; Pompeia, P.J. Dynamical Analysis of the Covarying Coupling Constants in Scalar–Tensor Gravity. *Symmetry* **2023**, *15*, 709. [CrossRef]
55. Teller, E. On the Change of Physical Constants. *Phys. Rev.* **1948**, *73*, 801. [CrossRef]
56. Chin, C.-W.; Stothers, R. Limit on the Secular Change of the Gravitational Constant Based on Studies of Solar Evolution. *Phys. Rev. Lett.* **1976**, *36*, 833. [CrossRef]
57. Sahini, V.; Shtanov, Y. Can a variable gravitational constant resolve the faint young Sun paradox. *Int. J. Mod. Phys. D* **2014**, *23*, 1442018. [CrossRef]
58. Morrison, L.V. Rotation of the Earth from AD 1663–1972 and the Constancy of G. *Nature* **1973**, *241*, 519–520. [CrossRef]
59. Sisterna, P.; Vucetich, H. Cosmology, oscillating physics, and oscillating biology. *Phys. Rev. Lett.* **1990**, *72*, 454–457. [CrossRef] [PubMed]
60. Benvenuto, O.G.; Althaus, L.G.; Torres, D.F. Evolution of white dwarfs as a probe of theories of gravitation: The case of Brans—Dicke. *Mon. Not. R. Astron. Soc.* **1999**, *305*, 905–919. [CrossRef]
61. Garcia-Berro, E.; Torres, S.; Renedo, I.; Camacho, J.; Althaus, L.G.; Córsico, A.H.; Salaris, M.; Isern, J. The white-dwarf cooling sequence of NGC 6791: A unique tool for stellar evolution. *Astron. Astrophys.* **2011**, *533*, A31. [CrossRef]
62. Córsico, A.H.; Althaus, L.G.; García-Berro, E.; Romero, A.D. An independent constraint on the secular rate of variation of the gravitational constant from pulsating white dwarfs. *J. Cosmol. Astropart. Phys.* **2013**, *2013*, 032. [CrossRef]
63. Degl'Innocenti, S.; Fiorentini, G.; Raffelt, G.G.; Ricci, B.; Weiss, A. Time-Variation of Newton's Constant and the Age of Globular Clusters. *Astron. Astrophys.* **1995**, *312*, 345–352.
64. Thorsett, S.E. The Gravitational Constant, the Chandrasekhar Limit, and Neutron Star Masses. *Phys. Rev. Lett.* **1996**, *77*, 1432. [CrossRef] [PubMed]
65. Bai, Y.; Salvado, J.; Stefanek, B.A. Cosmological constraints on the gravitational interactions of matter and dark matter. *J. Cosmol. Astropart. Phys.* **2015**, *10*, 029. [CrossRef]
66. Ooba, J.; Ichiki, K.; Chiba, T.; Sugiyama, N. Cosmological constraints on scalar–tensor gravity and the variation of the gravitational constant. *Prog. Theor. Exp. Phys.* **2017**, *4*, 043E03. [CrossRef]
67. Copi, C.J.; Davis, A.N.; Krauss, L.M. New Nucleosynthesis Constraint on the Variation of *G*. *Phys. Rev. Lett.* **2004**, *92*, 171301. [CrossRef]
68. Alvey, J.; Sabti, N.; Escudero, M.; Fairbairn, M. Improved BBN constraints on the variation of the gravitational constant. *Eur. Phys. J. C* **2020**, *80*, 148. [CrossRef]
69. Bellinger, E.P.; Christensen-Dalsgaard, J. Asteroseismic Constraints on the Cosmic-time Variation of the Gravitational Constant from an Ancient Main-sequence Star. *Astrophys. J. Lett.* **2019**, *887*, L1. [CrossRef]
70. Williams, J.G.; Turyshev, S.G.; Boggs, D.H. Progress in Lunar Laser Ranging Tests of Relativistic Gravity. *Phys. Rev. Lett.* **2004**, *93*, 261101. [CrossRef] [PubMed]
71. Hofmann, F.; Müller, J. Relativistic tests with lunar laser ranging. *Class. Quantum Gravity* **2018**, *35*, 035015. [CrossRef]
72. Pitjeva, E.V.; Pitjev, N. Relativistic effects and dark matter in the Solar system from observations of planets and spacecraft. *Mon. Not. R. Astron. Soc.* **2013**, *432*, 3431. [CrossRef]
73. Fienga, A.; Laskar, J.; Exertier, P.; Manche, H.; Gastineau, M. Tests of General relativity with planetary orbits and Monte Carlo simulations. *arXiv* **2014**, arXiv:1409.4932. [CrossRef]
74. Genova, A.; Mazarico, E.; Goossens, S.; Lemoine, F.G.; Neumann, G.A.; Smith, D.E.; Zuber, M.T. Solar system expansion and strong equivalence principle as seen by the NASA MESSENGER mission. *Nat. Commun.* **2018**, *9*, 289. [CrossRef] [PubMed]
75. Damour, T.; Gibbons, G.W.; Taylor, J.H. Limits on the variability of G using binary-pulsar data. *Phys. Rev. Lett.* **1988**, *61*, 1151–1154. [CrossRef] [PubMed]
76. Kaspi, V.M.; Taylor, J.H.; Ryba, M. High-Precision Timing of Millisecond Pulsars. III. Long-Term Monitoring of PSRs B1855+09 and B1937+21. *Astrophys. J.* **1994**, *428*, 713. [CrossRef]
77. Zhu, W.W.; Desvignes, G.; Wex, N.; Caballero, R.N.; Champion, D.J.; Demorest, P.B.; Ellis, J.A.; Janssen, G.H.; Kramer, M.; Krieger, A.; et al. Tests of gravitational symmetries with pulsar binary J1713+0747. *Mon. Not. R. Astron. Soc.* **2019**, *482*, 3249–3260. [CrossRef]
78. Gaztañaga, E.; García-Berro, E.; Isern, J.; Bravo, E.; Domínguez, I. Bounds on the possible evolution of the gravitational constant from cosmological type-Ia supernovae. *Phys. Rev. D* **2001**, *65*, 023506. [CrossRef]

79. Wright, B.S.; Li, B. Type Ia supernovae, standardizable candles, and gravity. *Phys. Rev. D* **2018**, *97*, 083505. [CrossRef]
80. Einstein, A. Über die vom Relativitätsprinzip geforderte Trägheit der Energie. *Ann. Phys.* **1907**, *328*, 371–384. [CrossRef]
81. Dicke, R.H. Gravitation without a Principle of Equivalence. *Rev. Mod. Phys.* **1957**, *29*, 363. [CrossRef]
82. Petit, J.-P. An interpretation of cosmological model with variable light velocity. *Mod. Phys. Lett. A* **1988**, *3*, 1527–1532, ibid 1733; ibid 2201. [CrossRef]
83. Moffat, J.W. Superluminary universe: A possible solution to the initial value problem in cosmology. *Int. J. Mod. Phys. D* **1993**, *2*, 351–365. [CrossRef]
84. Moffat, J.W. Quantum gravity, the origin of time and time's arrow. *Found. Phys.* **1993**, *23*, 411–437. [CrossRef]
85. Albrecht, A.; Magueijo, J. Time varying speed of light as a solution to cosmological puzzles. *Phys. Rev. D* **1999**, *59*, 043516. [CrossRef]
86. Barrow, J.D. Cosmologies with varying light speed. *Phys. Rev. D* **1999**, *59*, 043515. [CrossRef]
87. Avelino, P.P.; Martins, C.J.A.P. Does a varying speed of light solve the cosmological problems? *Phys. Lett. B* **1999**, *459*, 468–472. [CrossRef]
88. Avelino, P.P.; Martins, C.J.A.P.; Rocha, G. VSL theories and the Doppler peak. *Phys. Lett. B* **2000**, *483*, 210–216. [CrossRef]
89. Moffat, J.W. Variable speed of light cosmology, primordial fluctuations and gravitational waves. *Eur. Phys. J. C* **2016**, *76*, 130. [CrossRef]
90. Lovyagin, N.; Raikov, A.; Yershov, V.; Lovyagin, Y. Cosmological Model Tests with JWST. *Galaxies* **2022**, *10*, 108. [CrossRef]
91. Scolnic, D.M.; Brout, D.; Carr, A.; Riess, A.G.; Davis, T.M.; Dwomoh, A.; Jones, D.O.; Ali, N.; Charvu, P.; Chen, R. The Pantheon+ Analysis: The Full Data Set and Light-curve Release. *Astrophys. J.* **2022**, *938*, 113. [CrossRef]
92. Brout, D.; Scolnic, D.; Popovic, B.; Riess, A.G.; Carr, A.; Zuntz, J.; Kessler, R.; Davis, T.M.; Hinton, S.; Jones, D.; et al. The Pantheon+ Analysis: Cosmological Constraints. *Astrophys. J.* **2022**, *938*, 110. [CrossRef]
93. Adams, N.J.; Conselice, C.J.; Ferreira, L.; Austin, D.; Trussler, J.; Juodžbalis, I.; Wilkins, S.M.; Caruana, J.; Dayal, P.; Verma, A.; et al. Discovery and properties of ultra-high redshift galaxies (9 < z < 12) in the JWST ERO SMACS 0723 Field. *arXiv* **2022**, arXiv:2207.11217.
94. Atek, H.; Shuntov, M.; Furtak, L.J.; Richard, J.; Kneib, J.-P.; Mahler, G.; Zitrin, A.; McCracken, H.J.; Charlot, S.; Chevallard, J.; et al. Revealing galaxy candidates at z∼9-16 with JWST observations of the lensing cluster SMACS J0723.3-7327. *arXiv* **2022**, arXiv:2207.12338.
95. Chen, Z.; Stark, D.P.; Endsley, R.; Topping, M.; Whitler, L. JWST/NIRCam Observations of Stars and HII Regions in z ≃ 6-8 Galaxies: Properties of Star Forming Complexes on 150 pc Scales. Charlot. *arXiv* **2022**, arXiv:2207.12657.
96. Donnan, C.T.; McLeod, D.J.; Dunlop, J.S.; McLure, R.J.; Carnall, A.C.; Begley, R.; Cullen, F.; Hamadouche, M.L.; Bowler, R.A.A.; Magee, D.; et al. The evolution of the galaxy UV luminosity function at redshifts z ~ 8–15 from deep JWST and ground-based near-infrared imaging. *arXiv* **2022**, arXiv:2207.12356. [CrossRef]
97. Finkelstein, S.L.; Bagley, M.B.; Haro, P.A.; Dickinson, M.; Ferguson, H.C.; Kartaltepe, J.S.; Papovich, C.; Burgarella, D.; Kocevski, D.D.; Huertas-Company, M.; et al. A Long Time Ago in a Galaxy Far, Far Away: A Candidate z ~ 12 Galaxy in Early JWST CEERS Imaging. *Astrophys. J. Lett.* **2022**, *940*, L55. [CrossRef]
98. Naidu, R.P.; Oesch, P.A.; van Dokkum, P.; Nelson, E.J.; Suess, K.A.; Brammer, G.; Whitaker, K.E.; Illingworth, G.; Bouwens, R.; Tacchella, S.; et al. Two Remarkably Luminous Galaxy Candidates at z ≈ 10–12 Revealed by JWST. *Astrophys. J. Lett.* **2022**, *940*, L14. [CrossRef]
99. Naidu, R.P.; Oesch, P.A.; Setton, D.J.; Matthee, J.; Conroy, C.; Johnson, B.D.; Weaver, J.R.; Bouwens, R.J.; Brammer, G.B.; Dayal, P.; et al. Schrodinger's Galaxy Candidate: Puzzlingly Luminous at at z ≈ 17, or Dusty/Quenched at z ≈ 5? *arXiv* **2022**, arXiv:2208.02794.
100. Ono, Y.; Harikane, Y.; Ouchi, M.; Yajima, H.; Abe, M.; Isobe, Y.; Shibuya, T.; Wise, J.H.; Zhang, Y.; Nakajima, K.; et al. Morphologies of Galaxies at z & 9 Uncovered by JWST/NIRCam Imaging: Cosmic Size Evolution and an Identification of an Extremely Compact Bright Galaxy at z ~ 12. *arXiv* **2022**, arXiv:2208.13582.
101. Tacchella, S.; Johnson, B.D.; Robertson, B.E.; Carniani, S.; D'Eugenio, F.; Kumar, N.; Maiolino, R.; Nelson, E.J.; Suess, K.A.; Üble, H.; et al. WST NIRCam+NIRSpec: Interstellar medium and stellar populations of young galaxies with rising star formation and evolving gas reservoirs. *arXiv* **2022**, arXiv:2208.03281.
102. Wu, Y.; Cai, Z.; Sun, F.; Bian, F.; Lin, X.; Li, Z.; Li, M.; Bauer, F.E.; Egami, E.; Fan, X.; et al. The Identification of a Dusty Multiarm Spiral Galaxy at z = 3.06 with JWST and ALMA. *arXiv* **2022**, arXiv:2208.08473. [CrossRef]
103. Yang, L.; Morishita, T.; Leethochawalit, N.; Castellano, M.; Calabro, A.; Treu, T.; Bonchi, A.; Fontana, A.; Mason, C.; Merlin, E.; et al. Early Results from GLASS-JWST. V: The First Rest-frame Optical Size–Luminosity Relation of Galaxies at z > 7. *Astrophys. J. Lett.* **2022**, *938*, L17. [CrossRef]
104. Baggen, J.F.W.; van Dokkum, P.; Labbe, I.; Brammer, G.; Miller, T.B.; Bezanson, R.; Leja, J.; Wang, B.; Withaker, K.E.; Suess, K.A. Sizes and mass profiles of candidate massive galaxies discovered by JWST at 7 < z < 9: Evidence for very early formation of the central ~100 pc of present-day ellipticals. *arXiv* **2023**, arXiv:2305.17162.

105. Carniani, S.; Hainline, K.; D'Eugenio, F.; Eisenstein, D.J.; Jakobsen, P.; Witstok, J.; Johnson, B.D.; Chevallard, J.; Maiolino, R.; Helton, J.M.; et al. Spectroscopic confirmation of two luminous galaxies at a redshift of 14. *Nature* **2024**, *633*, 318–322. [CrossRef]
106. van Dokkum, P.G.; Whitaker, K.E.; Brammer, G.; Franx, M.; Kriek, M.; Labbé, I.; Marchesini, D.; Quadri, R.; Bezanson, R.; Illing-worth, G.D.; et al. The growth of massive galaxies since z = 2. *Astrophys. J.* **2010**, *709*, 1018. [CrossRef]
107. Costantin, L.; P'erez-Gonz'alez, P.G.; Vega-Ferrero, J.; Huertas-Company, M.; Bisigello, L.; Buitrago, F.; Bagley, M.B.; Cleri, N.J.; Cooper, M.C.; Finkelstein, S.L.; et al. Expectations of the Size Evolution of Massive Galaxies at $3 \leq z \leq 6$ from the TNG50 Simulation: The CEERS/JWST View. *Astrophys. J.* **2023**, *946*, 71. [CrossRef]
108. Ormerod, K.; Conselice, C.J.; Adams, N.J.; Harvey, T.; Austin, D.; Trussler, J.; Ferreira, L.; Caruana, J.; Lucatelli, G.; Li, Q.; et al. EPOCHS VI: The size and shape evolution of galaxies since z ~ 8 with JWST Observations. *Mon. Not. R. Astron. Soc.* **2024**, *527*, 6110. [CrossRef]
109. Varadaraj, R.G.; Bowler, R.A.A.; Jarvis, M.J.; Adams, N.J.; Choustikov, N.; Koekemoer, A.M.; Carnall, A.C.; McLeod, D.J.; Dunlop, J.S.; Donnan, C.T.; et al. The sizes of bright Lyman-break galaxies at $z \simeq 3$–5 with JWST PRIMER. *arXiv* **2024**, arXiv:2401.15971. [CrossRef]
110. Westcott, L.; Conselice, C.J.; Harvey, T.; Austin, D.; Adams, N.; Ferrari, F.; Ferreira, L.; Trussler, J.; Li, Q.; Rusakov, V.; et al. EPOCHS XI: The Structure and Morphology of Galaxies in the Epoch of Reionization to z ~ 12.5. *arXiv* **2024**, arXiv:2412.14970. [CrossRef]
111. Yang, L.; Kartaltepe, J.S.; Franco, M.; Ding, X.; Achenbach, M.J.; Arango-Toro, R.C.; Casey, C.M.; Drakos, N.E.; Faisst, A.L.; Gillman, S.; et al. COSMOS-Web: Unraveling the Evolution of Galaxy Size and Related Properties at $2 < z < 10$. *arXiv* **2025**, arXiv:2504.07185.
112. Gupta, R.P. Evolution of Size, Mass, and Density of Galaxies Since Cosmic Dawn. *Galaxies* **2025**, *13*, 115. [CrossRef]
113. Gandolfi, G.; Rodighiero, G.; Castellano, M.; Fontana, A.; Santini, P.; Dickinson, M.; Finkelstein, S.; Catone, M.; Calabrò, A.; Merlin, E.; et al. Mysteries of Capotauro: Investigating the puzzling nature of an extreme F356W-dropout. *arXiv* **2025**, arXiv:2509.01664. [CrossRef]
114. Aghanim, N.; Akrami, Y.; Arroja, F.; Ashdown, M.; Aumont, J.; Baccigalupi, C.; Ballardini, M.; Banday, A.J.; Barreiro, R.B.; Bartolo, N.; et al. Planck 2018 results I. Overview and the cosmological legacy of Planck. *Astron. Astrophys.* **2020**, *641*, A1. [CrossRef]
115. Lodha, K.; Calderon, R.; Matthewson, W.L.; Shafieloo, A.; Ishak, M.; Pan, J.; Garcia-Quintero, C.; Huterer, D.; Valogiannis, G.; Ureña-López, L.A.; et al. Extended Dark Energy analysis using DESI DR2 BAO measurements. *arXiv* **2025**, arXiv:2503.14743. [CrossRef]
116. Velten, H.E.S.; vom Marttens, R.F.; Zimdahl, W. Aspects of the cosmological "coincidence problem". *Eur. Phys. J.* **2014**, *74*, 3160. [CrossRef]
117. Tolman, T. Relativity, Thermodynamics and Cosmology. *Int. Ser. Monogr. Phys.* **1934**, *18*, 327–328.
118. Gupta, R.P. Testing CCC+TL Cosmology with Galaxy Rotation Curves. *Galaxies* **2025**, *13*, 108. [CrossRef]
119. Daod, N.A.; Zeki, M.K. Density and Mass Distribution of Spiral Galaxy NGC 3198. *Astrophys. J.* **2019**, *870*, 107. [CrossRef]
120. Lelli, F.; McGaugh, S.S.; Schombert, J.M. SPARC: Mass Models for 175 Disk Galaxies with Spitzer Photometry and Accurate Rotation Curves. *Astron. J.* **2016**, *152*, 157. [CrossRef]
121. McGaugh, S.S. (Case Western Reserve University, Cleveland, Ohio, USA). Personal communication, 2024.
122. Hernquist, L. An Analytical Model for Spherical Galaxies and Bulges. *Astrophys. J.* **1990**, *356*, 359. [CrossRef]
123. Sanders, R.H.; Begeman, K.G. Modified dynamics (MOND) as a dark halo. *Mon. Not. R. Astron. Soc.* **1994**, *266*, 360–366. [CrossRef]
124. Li, P.; Lelli, F.; McGaugh, S.; Schombert, J. Fitting the radial acceleration relation to individual SPARC galaxies. *arXiv* **2018**, arXiv:1803.00022. [CrossRef]
125. Mandelbaum, R.; Seljak, U.; Cool, R.J.; Blanton, M.; Hirata, C.M.; Brinkmann, J. Density profiles of galaxy groups and clusters from SDSS galaxy–galaxy weak lensing. *Mon. Not. R. Astron. Soc.* **2006**, *372*, 758. [CrossRef]
126. van Dokkum, P.; Brammer, G.; Wang, B.; Leja, J.; Conroy, C. A massive compact quiescent galaxy at z = 2 with a complete Einstein ring in JWST imaging. *Nat. Astron.* **2024**, *8*, 119–125. [CrossRef]
127. Kong, D.; Yang, D.; Yu, H. Cold Dark Matter and Self-interacting Dark Matter Interpretations of the Strong Gravitational Lensing Object JWST-ER1. *Nat. Astron.* **2024**, *965*, L19. [CrossRef]
128. Oguri, M. Fast Calculation of Gravitational Lensing Properties of Elliptical Navarro-Frenk-White and Hernquist Density Profiles. *Astron. Soc. Pac.* **2021**, *133*, 074504. [CrossRef]
129. Koposov, S.E.; Casey, A.R.; Belokurov, V.; Lewis, J.R.; Gilmore, G.; Worley, C.; Hourihane, A.; Randich, S.; Bensby, T.; Bragaglia, A.; et al. Kinematics and chemistry of recently discovered reticulum 2 and horologium 1 dwarf galaxies. *Astrophys. J.* **2015**, *811*, 62. [CrossRef]
130. Simon, J.D.; Drlica-Wagner, A.; Li, T.S.; Nord, B.; Geha, M.; Bechtol, K.; Balbinot, E.; Buckley-Geer, E.; Lin, H.; Marshall, J.; et al. Stellar kinematics and metallicities in the ultra-faint dwarf galaxy reticulum II. *Astrophys. J.* **2015**, *808*, 95. [CrossRef]
131. Minor, Q.E.; Pace, A.B.; Marshall, J.L.; Strigari, L.E. Robust velocity dispersion and binary population modelling of the ultrafaint dwarf galaxy Reticulum II. *Mon. Not. R. Astron. Soc.* **2019**, *487*, 2961–2968. [CrossRef]

132. Comeron, S.; Trujillo, I.; Cappellari, M.; Buitrago, F.; Garduño, L.E.; Zaragoza-Cardiel, J.; Zinchenko, I.A.; Lara-López, M.A.; Ferré-Mateu, A.; Dib, S. The massive relic galaxy NGC 1277 is dark matter deficient From dynamical models of integral-field stellar kinematics out to five effective radii. *Astron. Astrophys.* **2023**, *675*, A143. [CrossRef]
133. Zwicky, F. On the Redshift of Spectral Lines Through Interstellar Space. *Proc. Natl. Acad. Sci. USA* **1929**, *15*, 773–779. [CrossRef]